Journal of Electrostatics 106 (2020) 103454

Contents lists available at ScienceDirect

Journal of Electrostatics

journal homepage: http://www.elsevier.com/locate/elstat

Experimental study on electrohydrodynamic flows of a dielectric liquid in a needle-plate configuration under direct/alternating current electric field

Zhihao Sun [a], Dexin Sun [a], Jinxin Hu [a], Philippe Traoré [b], Hong-Liang Yi [a], Jian Wu [a,*]

[a] Key Laboratory of Aerospace Thermophysics, School of Energy Science and Engineering, Harbin Institute of Technology, Harbin, 150001, PR China
[b] Institut PPRIME, Département Fluide-Thermique-Combustion, Boulevard Pierre et Marie Curie, BP 30179, 86962, Futuroscope-Chasseneuil, France

ARTICLE INFO

Keywords:
Electrohydrodynamics
Electroconvection
Particle image velocimetry
Needle-plate geometry
Dielectric liquid

ABSTRACT

Experiments on the electrohydrodynamic (EHD) flow characteristics of a dielectric liquid in a sharp needle-plate configuration under direct current (DC) and alternating current (AC) electric field are carried out. The current-voltage characteristics and the velocity field are simultaneously recorded for understanding the flow behavior and its mechanism. For the DC case, a critical voltage separating the conduction and injection regimes and the corresponding flow reverse is observed. Results indicate the polarity of voltage only influences the flow's intensity in the injection regime. For the AC case, two types of signals with the same 50% duty cycle are considered. For the pulsed voltage (−2.0kV to 0), the flow generally keeps the plume structure and shows weaker strength than the corresponding DC case. For the AC signal (-2.0kV–+2.0kV), the velocity amplitude first decreases and then tends to be constant with the increase of frequency. The weak flow motion with high frequency AC field is due to conduction.

1. Introduction

Electrohydrodynamics (EHD) mainly studies the interaction between electric field and different fluid media [1,2]. The flow of single-phase dielectric liquids driven by electric body force (i.e. electroconvection) is a typical and fundamental EHD phenomenon. The electric force includes three components, namely, Coulomb force, dielectrophoretic force and electrostriction force. In most cases, the Coulomb force that is due to the electric field exerting on free space charge plays a dominant role [3]. For isothermal dielectric liquids, there are two major mechanisms for the generation of free space charges: conduction and charge injection [4–6]. For conduction, electric field causes the imbalance in the dissociation-recombination equilibrium, which leads to the generation of the net charge. The positive and negative ions produced due to dissociation are attracted to the electrodes of opposite polarities, and a heterocharge layer is formed in the electrode vicinity. When the electrodes are asymmetrical, the Coulomb force can drive the flow moving towards the electrode with larger curvature [7,8]. The charge injection is related to the electrochemical reaction that takes place at the interface between electrode and dielectric liquid [9]. The accumulation of charges on the surface of the electrode results in the formation of a homocharge layer with the same polarity as the electrode. When subjected to the external electric field, the homocharge layer of ions is repelled away from the electrode and injected into the bulk liquid. The charge carrying the surrounding fluid forms a flow moving away from the injecting electrode. Both injection-driven and conduction-driven convection of dielectric liquids with asymmetrical electrodes has been observed and investigated by experiments and numerical simulations [5,6,10–15]. The pumps based on both types of charge generation mechanisms, i.e. ion-drag pumping and conduction pumping have been proposed and extensively studied [4].

For the experimental studies of electroconvection of dielectric liquids, Atten et al. examined the flow structure induced by charge injection from a needle with small radius theoretically and experimentally [16]. They also proposed a conduction model for the asymmetric needle-plate configuration for the first time, which establishes the foundation for the research of EHD conduction pumps [7]. In the earlier research with electroconvection of dielectric liquids, the Schlieren system was widely used for the visualization of flow pattern [17]. Later, the Laser Doppler Velocimetry (LDV) and Particle Image Velocimetry (PIV) systems have been used to record the flow velocity, which provides great help in the analysis of flow mechanism and bifurcation phenomena [18,19]. A series of experiments with electroconvection in the blade-plane configuration have been performed by Louste and his colleagues [5,

* Corresponding author.
E-mail address: jian.wu@hit.edu.cn (J. Wu).

https://doi.org/10.1016/j.elstat.2020.103454
Received 10 October 2019; Received in revised form 18 March 2020; Accepted 25 March 2020

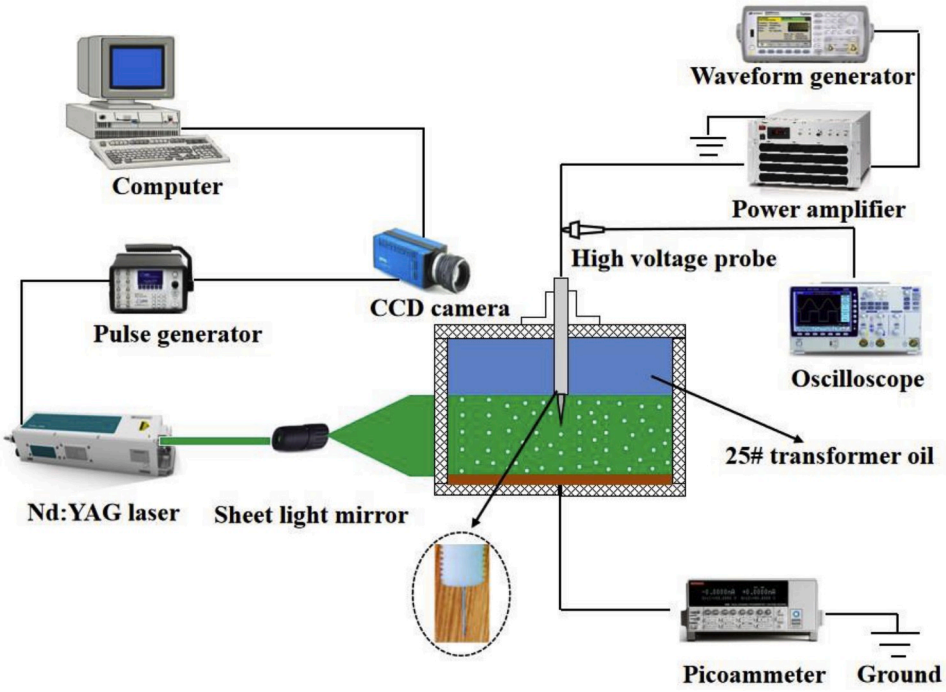

Fig. 1. Schematic diagram of the experimental setup.

13,18–20]. Since they mainly considered strong Direct Current (DC) electric fields, injection is the source for the free charges in their experiments. Testi et al. experimentally explored the application of injection-induced convection in needle-plate configuration for active heat transfer enhancement [10,11]. However, the authors did not measure the flow velocity but focused on the heat transfer performance. Chirkov et al. performed a systematic study on electroconvection in the needle-plate configuration based on the injection-conduction model [6, 14,21]. In particular, they recently designed a novel EHD system, in which solid dielectric material is used to form strong local electric field far away from the electrodes, and then the flow motion is caused by field-enhanced dissociation solely [14]. We highlight that all above mentioned experimental results are for the DC electric field.

In two recent studies, Louste et al. used the PIV technique to investigate the transition from conduction to injection with DC field and blade/cylinder-plane electrode configuration [5,20]. Very complicated flow patterns have been observed, especially in the regime with relatively weak electric field. This is inherently related to the coexistence of both injection and conduction mechanism for free charges, and their complex relationship with the electric field. On the other hand, there are limited experimental studies for electroconvection of dielectric liquids with Alternating Current (AC) electric field [22]. In the early study [23], Atten extended their previous study of DC electroconvecion between parallel plates to AC field. They mainly focused on the influence of the frequency on the linear stability criterion. Daaboul et al. studied the transient velocity field of dielectric liquids subjected to an AC square wave signal, with different frequencies [13]. They considered the blade-plate configuration and high voltage (±30.0kV) was applied. The injection served as the sole source for free ions in this study. It should be noted that there is a class of research focusing on electroconvection solely driven by dielectrophoretic force. To this end, AC electric field with high frequency is often used to avoid charge injection and the consequent Coulomb force. However, AC electric field with low frequency may show strong influence in both single-phase and multi-phase electro-thermal systems [24–26].

In this paper, a preliminary experiment on the EHD flow characteristics of a dielectric liquid in a needle-plate configuration under DC and AC field is performed. The electric current-voltage characteristics and the velocity field are simultaneously recorded to gain deep understanding of the charge generation mechanism and its interaction with the flow and electric fields. While the needle-plate configuration has a confined injection region, in the blade-plate geometry the injection can be initiated at different points on the blade. The resulting flow structures are different. Instead using a high voltage as [13], a relatively low voltage is considered and then conduction may play an important role in our study. In addition, to help understand the results with AC square signal, we also perform the experiments with the pulsed voltages. The remainder of this paper is organized as follows. In Section 2, the experimental setup, dielectric liquid, electrical apparatus, and the PIV system are introduced. In Section 3, the DC and AC experimental results are discussed. Finally, the conclusions are drawn in the last section.

Table 1
Physical properties of the mixture (25# transformer oil with 10% cyclohexanol alcohol) at 20 °C.

Parameter	Symbol	Value
Mass density	ρ	900.0 kg/m^3
Conductivity	σ	4.37×10^{-11} S/m
Relative permittivity	ε	2.16
Kinematic viscosity	ν	8.24×10^{-6} m^2/s

2. Experimental set-up

2.1. Electrical apparatus

Fig. 1 shows the schematic diagram of experimental setup. The experimental cell is a polymethylmethacrylate (PMMA) cubical cavity with the internal size of 140.0 mm × 140.0 mm × 140.0 mm. The cavity is filled with the mixture of 25# transformer oil with 10% cyclohexanol alcohol by volume. By mixing cyclohexanol alcohol, the conductivity of oil increases from 4.65×10^{-12} S/m to 4.37×10^{-11} S/m. The field-enhanced dissociation effect is negligible when the conductivity is less than 10^{-11} S/m [6]. When the conductivity is between 10^{-11} S/m and 10^{-8} S/m, both conduction and injection mechanisms should be taken into consideration. For the fluid mixture, the parameters including the

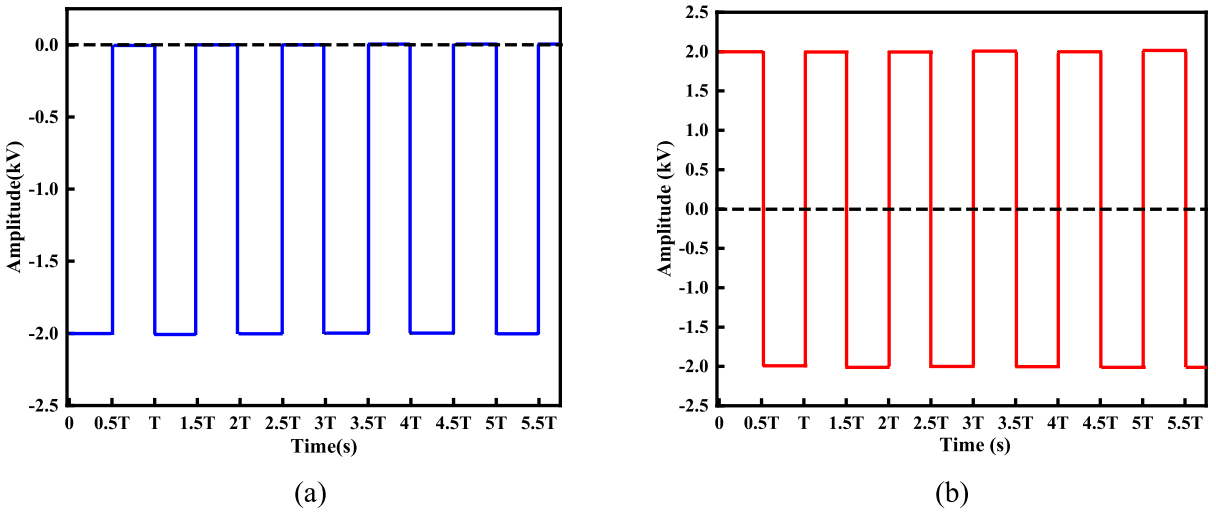

Fig. 2. AC voltage waveform: (a) −2.0 kV to 0 square wave (b) ±2.0 kV square wave.

conductivity, permittivity, density and viscosity are measured by laboratory apparatuses and summarized in Table 1.

An iron plate electrode with the size of 138.0 mm × 138.0 mm × 1.0 mm(thickness) is placed horizontally at the bottom of the cavity and grounded. A sharp stainless steel needle with diameter of 1.2mm is placed vertically above the plate. The distance between the two electrodes is fixed at 15.0mm, and the curvature of needle is estimated to be about 0.1mm. The needle electrode is connected to the high voltage power supply.

The DC and AC voltage are supplied by a waveform generator (Keysight Tech., MODEL 33512B, USA) and a high voltage amplifier (Matsusada, AMP-30B10, Japan). A high voltage probe (Tektronix, P6015A, USA) and an oscilloscope (Tektronix, MSO54, USA) are connected to the circuit to monitor the actual output voltage. The electric current in the circuit is measured by a picoammeter (Keithley, 6482, USA).

In our experiments, it is observed that for the present sharp needle and the distance between needle and plate mentioned above a stable charged jet structure can be formed when the applied DC voltage beyond 2.0kV. The charged jet structure will be shown and analyzed in Section 3. For low voltages that lie in the conduction regime, the corresponding flow patterns are irregular. On the other hand, if the amplitude of the applied voltage is increased, the flow between the electrodes would no longer be stable and a chaotic flow is observed. Therefore, as a starting point, the amplitude of AC voltage is fixed as 2.0kV in this study. The waveform of the AC voltage in 1.0 second is shown in Fig. 2, in which the duty cycle is 50%. The symbol T is the period of the AC voltage, and the frequency $f = 1/T$. The influence of voltage amplitude, waveform and duty cycle can be a working direction for future study.

2.2. Particle image velocimetry system

The velocity fields are recorded by a self-assembly 2D2C PIV system. The PIV technology requires seeding particles to be dispersed in the fluid and illuminated by laser, and the instantaneous position of particles is recorded by camera. The illumination is realized by the double-pulsed Nd:YAG laser (Beamtech, Vlite-380, China) with a pulse energy of 380.0mJ at a wavelength of 532.0nm. A 14-bit CCD camera (CookeCorp, PCO 2000, Germany) is used for the image acquisition. The double-pulsed Nd:YAG laser and the CCD camera are connected to a synchronizer (Berkeley Nucleonics, Model 577, USA). The sampling frequency of PIV system is set to 4.0Hz. This frequency has been verified with the Nyquist sampling theorem. Based on tests, we take 1000 pairs of images for each experimental condition to obtain statistical convergence results.

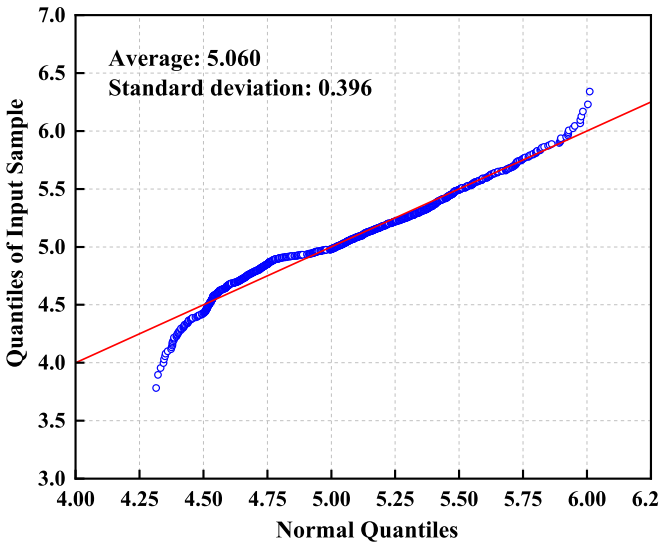

Fig. 3. Q-Q plot distribution for velocity values at −2.0 kV.

To obtain reliable velocity measurement results, the density and electrical properties of the seeding particles should be close to the dielectric liquid [27]. In this study, SiO_2 particle with average diameter of 5.0μm is chosen, and the concentration of 0.0072 g/L is used.

During the experiments, the Quantile-Quantile (Q-Q) Plot method [28] is adopted to investigate the accuracy of velocity value measured by the PIV system. The Q-Q plot is a graphical technique to test if two sets of data plausibly obey same distribution. The experimental data were compared with normal distribution. If each set of experimental data was distributed around a straight line, it would be concluded that the experimental results obey normal distribution. From the straight line ($y = ax + b$), the average value of experimental results was known as $-b/a$, the standard deviation was known as $-1/a$ [29].

Fig. 3 plots the Q-Q distribution for 1000 velocity values of the intermediate point between needle-plate electrodes (x = 20.0mm, y = 8.5mm) when the applied DC voltage is -2.0kV. It can be seen that each velocity value computed from a pair of images locates around a straight line, which means the velocity values obey the normal distribution. In this representative case, the average value $\overline{V}_{DC}$and standard deviation σ_{DC} are 5.060 mm/s and 0.396 mm/s, respectively. The 99.7% confidence interval is calculated from the following formula:

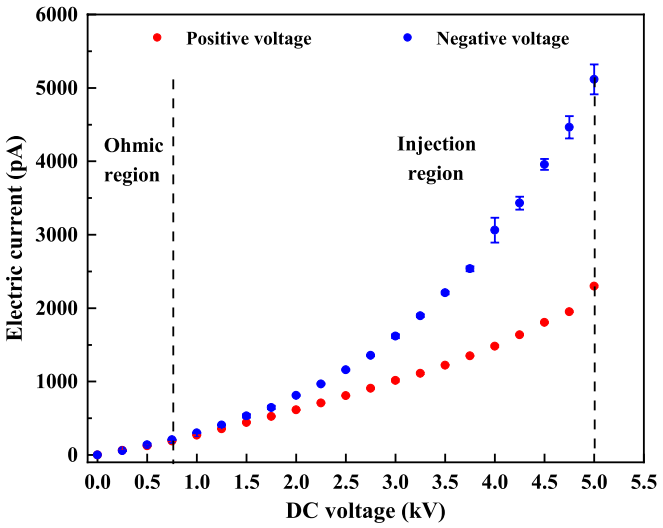

Fig. 4. Current-voltage characteristics for DC electric field.

$$\overline{V} \pm \frac{3\sigma}{\sqrt{n}} = 5.060 \pm 0.038 \quad mm/s \tag{1}$$

where n is the number of sampling points. Therefore, the relative error can be calculated as:

$$\text{error} = \frac{3\sigma}{\sqrt{n}} \frac{1}{\overline{V}} = 0.74\% \tag{2}$$

The measurement accuracy is analyzed for all experimental conditions, and the maximum relative error of the velocity average value is less than 5.0% with 99.7% confidence interval.

3. Results and discussion

3.1. Electroconvection with DC electric field

We first consider the DC electric field, and the influence of voltage magnitude and polarity is investigated. The transition from conduction to injection regimes is highlighted. The information of voltage-current characteristics and fluid velocity is simultaneously recorded for analysis.

3.1.1. Voltage-current characteristics

In Fig. 4, we present the DC voltage-current curve. In experiments, we noticed that the electric current never reaches a steady state but continuously changes with time. So for each point the electric current is average value based on the results recorded for sufficiently long time. It can be observed that the DC voltage-current curve can be roughly divided into two regions, namely the Ohmic region and the injection region. The range for the Ohmic region is found to lie between 0 and 0.75 kV. In this range, the current increases linearly with the applied positive or negative DC voltage. The order of current in this region depends on the liquid's conductivity. There is only slight difference between the electric currents with positive and negative voltages. In the injection region, the applied voltage is above 0.75 kV, and a large amount of charges are injected into the liquid and consequently the current rapidly increases with voltage. In the injection region, for the same voltage the electric current with negative polarity is higher than the positive one. In addition, the difference between the two electric current curves increases with the applied voltage. For instance, the electric currents are 2300.3 pA and 5117.2 pA with +5.0 kV and −5.0 kV, respectively. By checking the plot-plot data format, the values of the exponents of V in the injection regions are 2.3 and 1.7 for the negative and positive polarities, respectively.

In [30], the authors presented the current-voltage characteristic for silicone oil in the blade-plate configuration, and they showed the data in the log-log format. In another study [31], the current-voltage characteristic for a needle-plate configuration and transformer oil is presented. Our present findings show the same tendency as [30,31]. We have not

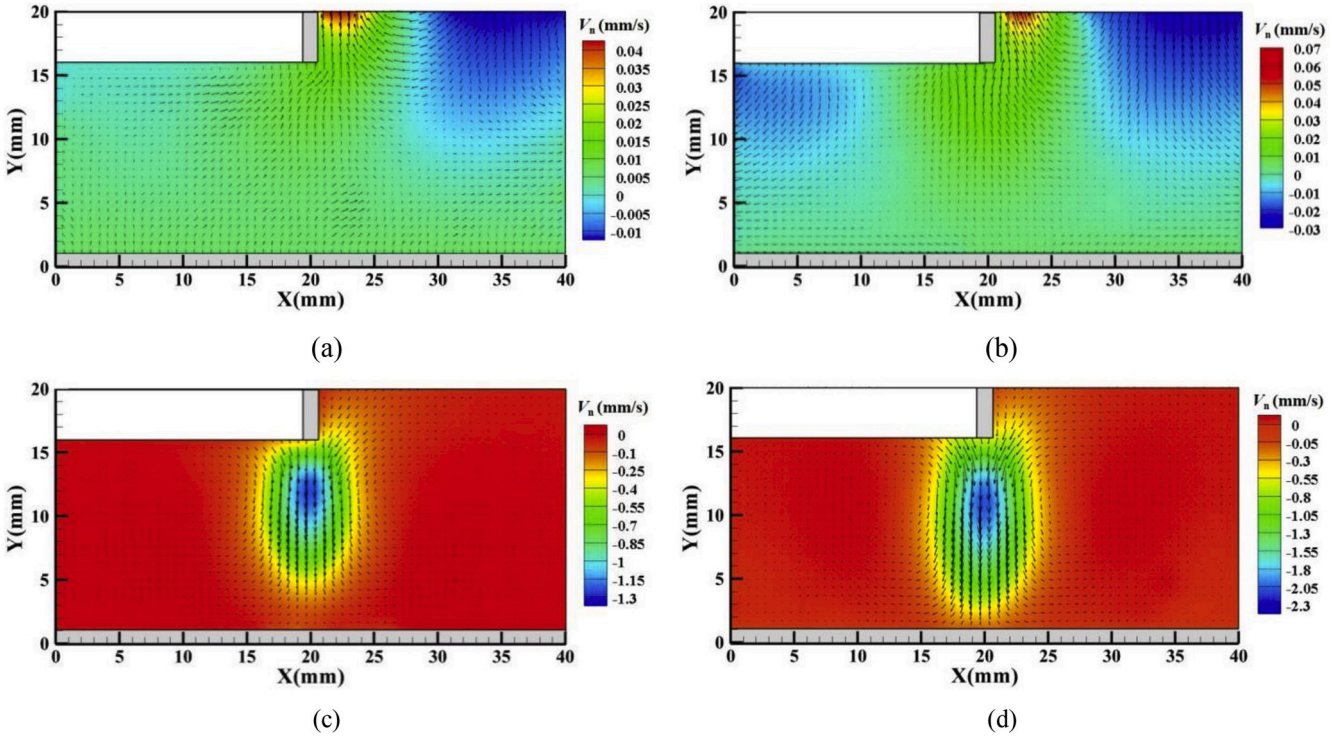

Fig. 5. Velocity contours and vectors with positive DC voltage: (a) 0.50 kV (b) 0.75 kV (c) 1.0 kV (d) 2.0 kV.

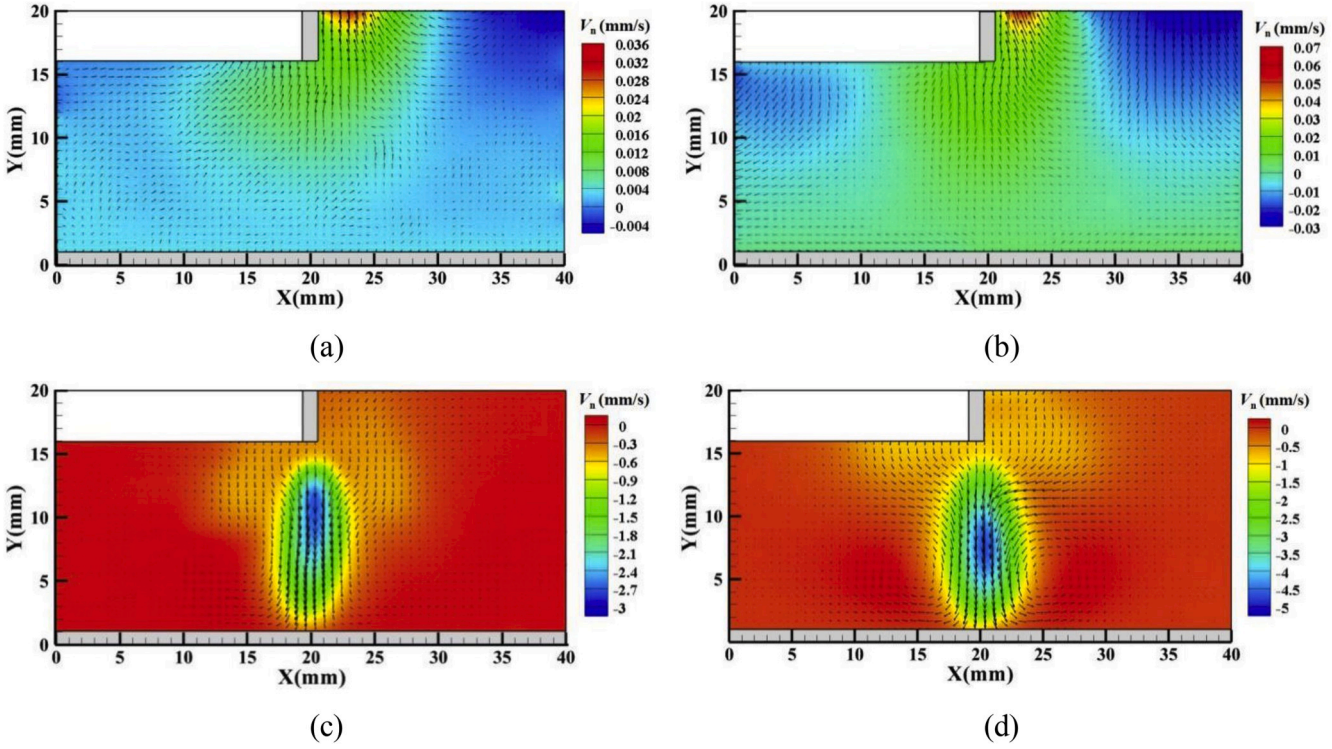

Fig. 6. Velocity contours and vectors with negative DC voltage: (a) −0.5tkV, (b) −0.75kV, (c) −1.0kV, (d) −2.0kV.

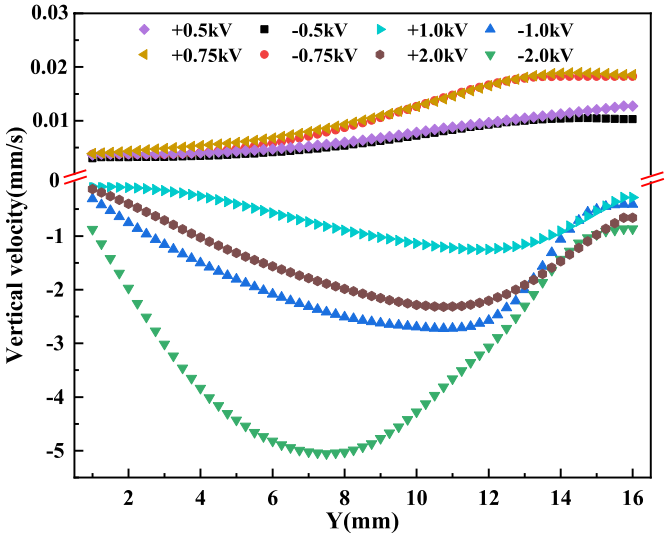

Fig. 7. Vertical velocity between the needle and plate electrodes for DC electric field.

observed a distinct saturation region but an intermediate region. In addition, we noticed that some points on the curve of negative voltage show obvious error bar. Two possible reasons include the unstable charge injection and the irregular flow motion. It is well-known that charge injection with bare metallic electrode is very sensitive to electrode. In our experiments, since the needle is not that sharp, the charge injection area and strength also increases along with the increase of applied voltage. However, this aspect is difficult to directly judge from experiments. For the flow motion, we observed that the structure of charged plume was regular and symmetrical when the applied voltage is small. For high voltage, the velocity of charged plume becomes much stronger, and the flow is unsteady with significant fluctuations and the structure of charged plume is irregular. This kind of flow can cause fluctuations in electric current. However, considering the amplitude of flow motion is still small, it may only plays a minor role.

3.1.2. *PIV velocity fields*

The PIV technique is used to record the velocity field for better understanding EHD flow characteristics. The velocity vectors and contours of the vertical velocity component $\boldsymbol{V_n}$ with eight sets of voltages in the range [-2.0kV, +2.0kV] are presented in Figs. 5 and 6. From the above analysis with the current-voltage characteristics, the transition between conduction and injection takes places in this range. The blank area without any data is due to the shadow of the needle when the laser is illuminated. Fig. 7 plots the distribution of the vertical velocity component along the center line connecting the tip of the shape electrode and the opposite plate.

For ±0.5 kV (Figs. 5a and 6a) and ±0.75 kV (Figs. 5b and 6b), it is found that the liquid moves towards the needle electrode. More precisely, as shown in Fig. 7, the vertical velocity takes positive value in the ranges of 1.0–16.0mm between the needle and plate electrodes. This flow pattern can be explained by the conduction mechanism. However, the velocity amplitude is fairly weak, which is due to the small amount of free charges considering the low conductivity (4.37×10^{-11} S/m) of dielectric liquid. As shown in Fig. 7, for the absolute applied voltage $|V| = 0.5$ and 0.75, the velocity curves almost coincide with each other for each case. This is consistent with the current-voltage characteristics.

As the applied voltage is increased to 1.0kV (Figs. 5c and 6c), we observed that the direction of liquid's motion reversed. That is, the liquid moves from the needle towards the plate electrode. Such reversal has been observed in the recent studies with the blade/cylinder-plate configurations [20,50]. This reverse is also intuitively shown by the sign change of velocity in Fig. 7. This phenomenon can be explained by the injection mechanism. From our experiments, the transition between conduction and injection takes place between 0.75 kV and 1.0kV, and the results seem to indicate that the polarity does not influence the transition range of voltage.

When the amplitude of applied DC voltage is further increased to

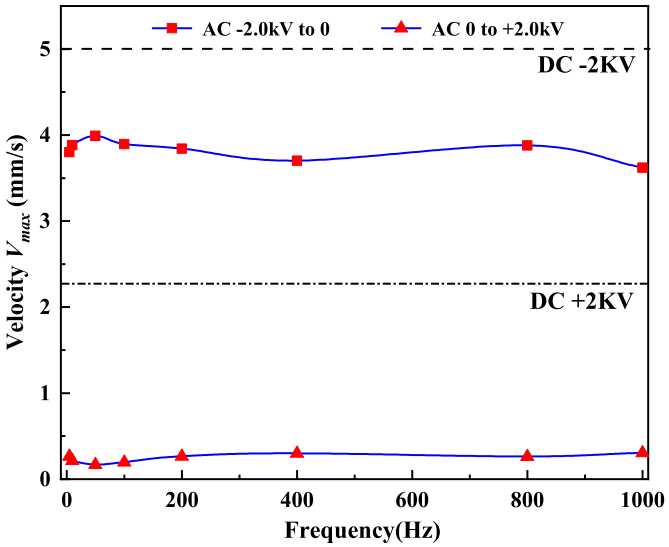

Fig. 8. The maximum velocity of charged plume versus frequency with pulsed voltage.

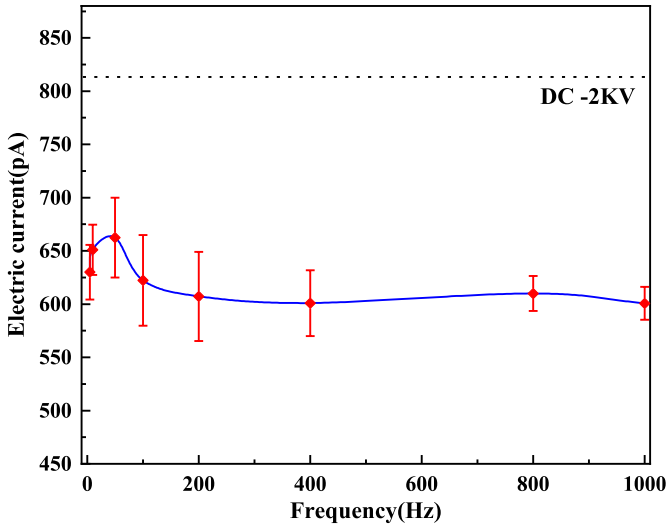

Fig. 9. The mean electric current versus frequency for the negative pulsed voltage.

2.0kV (Figs. 5d and 6d), the velocity amplitude dramatically increases due to charge injection. In addition, the velocity field with negative polarity is stronger than positive polarity (see Fig. 7), a phenomenon that has been frequently observed in previous experiments with dielectric liquids and gas discharge. For instance, the maximum velocities of charged plume are 2.31 mm/s and 5.06 mm/s with the applied +2.0 kV and −2.0 kV, respectively. Since free charges can be transported by flow motion, the difference in the fluid velocity for positive and negative polarity is one of the sources for the difference with the current-voltage characteristics in the injection regime. However, compared to other sources (such as the injection laws with different polarities and the motilities with the positive and negative ions), its relative contribution needs more research. By rotating the camera, we observed that the velocity field of impinging charged plume shows axis-symmetrical structure. For the 2D cross-section, as shown in Figs. 5d and 6d the flow divides into two sides and forms two counter-rotating vortices on each side before reaching the plate electrode. The flow shows similar characteristics of the classical impinging jet flow [12,13,17].

3.2. Electroconvection with AC electric field

Then we consider the AC electric field. To simplify the discussion, we only consider ±2.0kV, at which the injection mechanism plays the dominant role. Two kinds of waveform shown in Fig. 2 are studied and the influence of frequency is highlighted.

3.2.1. Applied −2.0kV to 0 and 0 to +2.0kV square waves

In Fig. 8, we present the maximum velocity of charged plume with pulsed signal (−2.0kV to 0 and 0 to +2.0kV) square wave at different frequencies. The frequency varies between 5.0 and 1000.0Hz. All results are statistical average values. For each polarity, the flow between the needle-plate electrodes is continuous for all frequencies tested. It is noticed that the maximum velocity of flow field is smaller than the corresponding values with the DC voltages, which are expressed with dash lines in Fig. 8.

For positive voltage, the flow field drops down to a fairly small value. By checking the PIV results and the current-voltage characteristics for this case (not shown here), a very irregular pattern was observed. One possible reason is that the injected charges reduce the local electric field around the sharp electrode. The injection area and strength is decreased. Then both injection and conduction mechanisms play important roles,

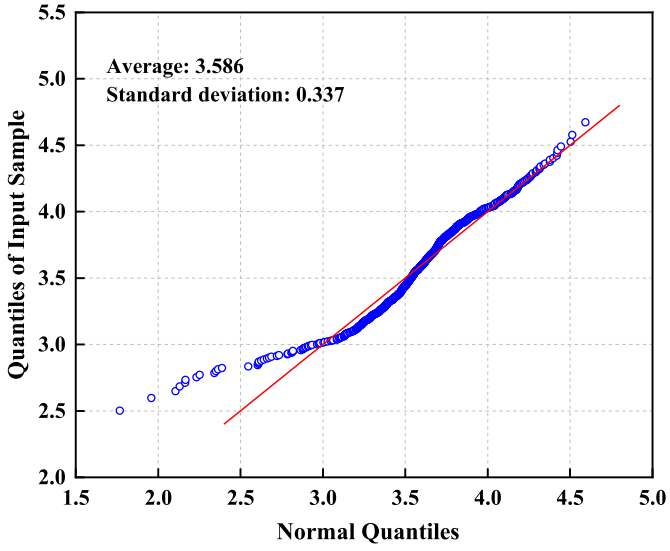

Fig. 10. The Q-Q plot distribution for velocity value with negative pulsed voltage and frequency 1000.0Hz.

and complex behavior occurs due to their interaction. However, more experiments are required to clarify the reason.

Here we focus on the results with the negative pulsed signal (−2.0 kV to 0). Fig. 9 shows the variation of the mean electric current with the frequency. For low frequencies ($f \leq 100.0$Hz), there is a hump, same as the velocity shown in Fig. 8. For high frequencies, both electric current and fluid velocity tend to constant values. The decrease in the maximum velocity with the negative pulsed voltage may be understood from two aspects. First, the effective acting time and the amount of injected charges are reduced by half, which means the average driving Coulomb force is smaller. Secondly, a full cycle is divided into two separate stages depending on the action of electric field or not. For the stage with imposed electric field, charges transport with both the drift and convection mechanisms. For the other stage, charges solely transport with the flow field. The change in the transport mechanism of charge influences the charge distribution, and consequently the electrical torque decreases and the resulting flow convection become weaker. However, quantitative evaluation with the contribution of the second aspect to the decrease in the velocity with frequency is challenging, and the direct

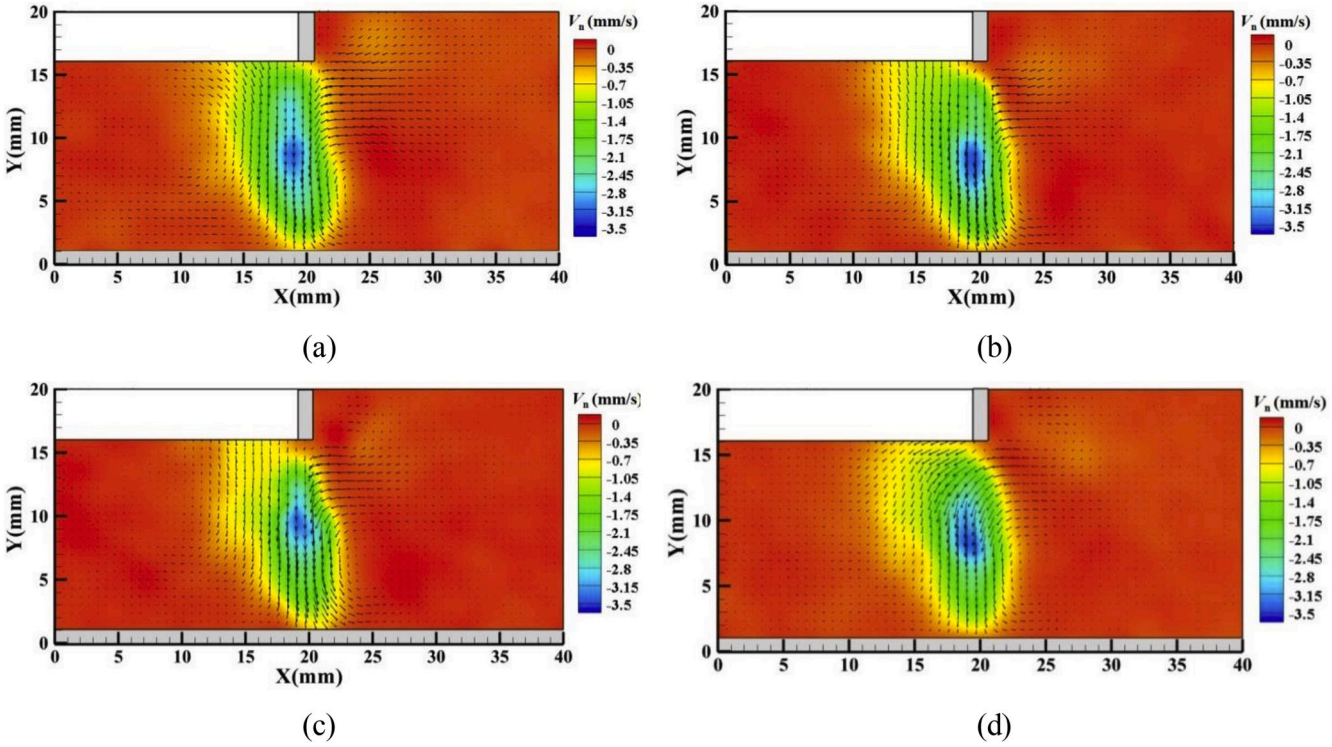

Fig. 11. Velocity field at different times with the −2.0kV to 0 square wave frequency of 1000.0Hz: (a) 100.0s, (b) 150.0s, (c) 200.0s, (d) 250.0s.

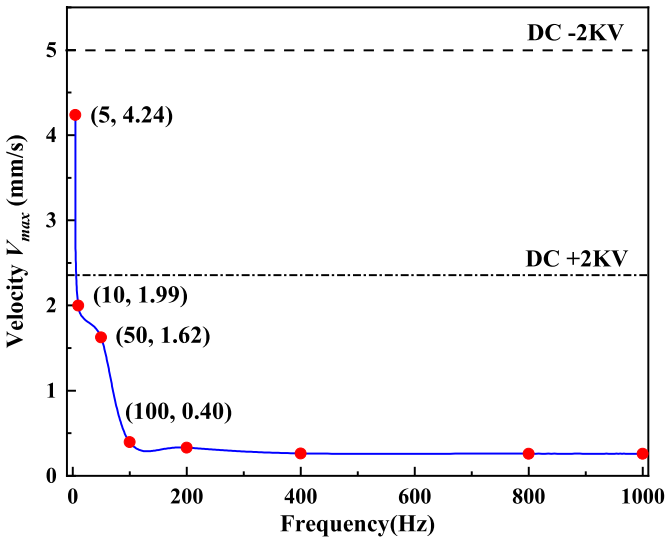

Fig. 12. Maximum velocity of charged plume with ±2.0 kV square wave frequency.

numerical simulation approach may provide help.

In Fig. 10, the charged plume velocity values of the intermediate point (x = 20.0mm, y = 8.5 mm) between the needle and plate electrodes with frequency 1000.0Hz are extracted and drawn by the means of Q-Q plot distribution. It shows that the data follow the normal distribution. The average value $\overline{V}_{AC}$ and standard deviation σ_{AC} are 3.59 mm/s and 0.34 mm/s, respectively. According to formula (2), the relative error under the applied frequency of 1000.0Hz is 0.89%.

In Fig. 11, the velocity field at different moments with the voltage of −2.0kV and the frequency of 1000.0Hz is shown. It is found that the flow always exists during the whole measurement time and generally keeps a plume structure. However, comparing to the structure under the same applied DC voltage, the charge plume with AC field becomes unsteady and asymmetrical. By rotating the camera, we observe that the flow field losses its axisymmetric characteristic and shows 3D structure. The asymmetrical 3D flow pattern has been widely observed in the previous studies of electroconvetion induced by the DC field with relatively low strength [5,20].

3.2.2. *Applied −2.0kV to +2.0kV square wave*

In this subsection, we consider the case of alternating polarity that is shown with Fig. 2b. In Fig. 12, we present the maximum velocity of charged plume with ±2.0 kV square wave at different frequencies. Each maximum velocity is extracted from 1000 sets of PIV velocity field. It shows that the maximum velocity of charged plume decreases along with the increase of the frequency. When frequency is 5.0Hz, the maximum velocity is 4.24 mm/s, within the range between the maximum velocities with the DC +2.0kV and DC -2.0kV. As the frequency increases, the maximum velocity dramatically decreases. For even higher frequency, say $f \geq$ 100.0Hz, the fluid hardly moves. This phenomenon is consistent with the observation by Daaboul et al. [13]. In their study, experiments were performed with a blade-plate configuration and ±30.0kV AC electric field, and therefore their peak velocity magnitude is much high than our present results.

To understand the fairly weak motion with high frequencies, two aspects should be considered. First of all, for the injection mechanism, there exits some critical frequency that separates two situations. For low frequency, the injected charges can enter into the bulk liquid and the Coulomb force can drive the flow motion. For high frequency, the injected charges do not have enough time to escape from the needle electrode before attracting back due to the reverse of the electric field, so the majority of injected charges remain in the region close to the emitter electrode [22]. This critical frequency should be compared with the ionic transit time $t_T = d/KE_0$, d being the distance between the needle and plate electrodes, K the ionic mobility, E_0 the electric field computed with no space charges [23]. For the liquid and electrode geometry considered in this study, we can estimate the critical frequency to be of the order 10. However, there is a small mechanical impulse from the

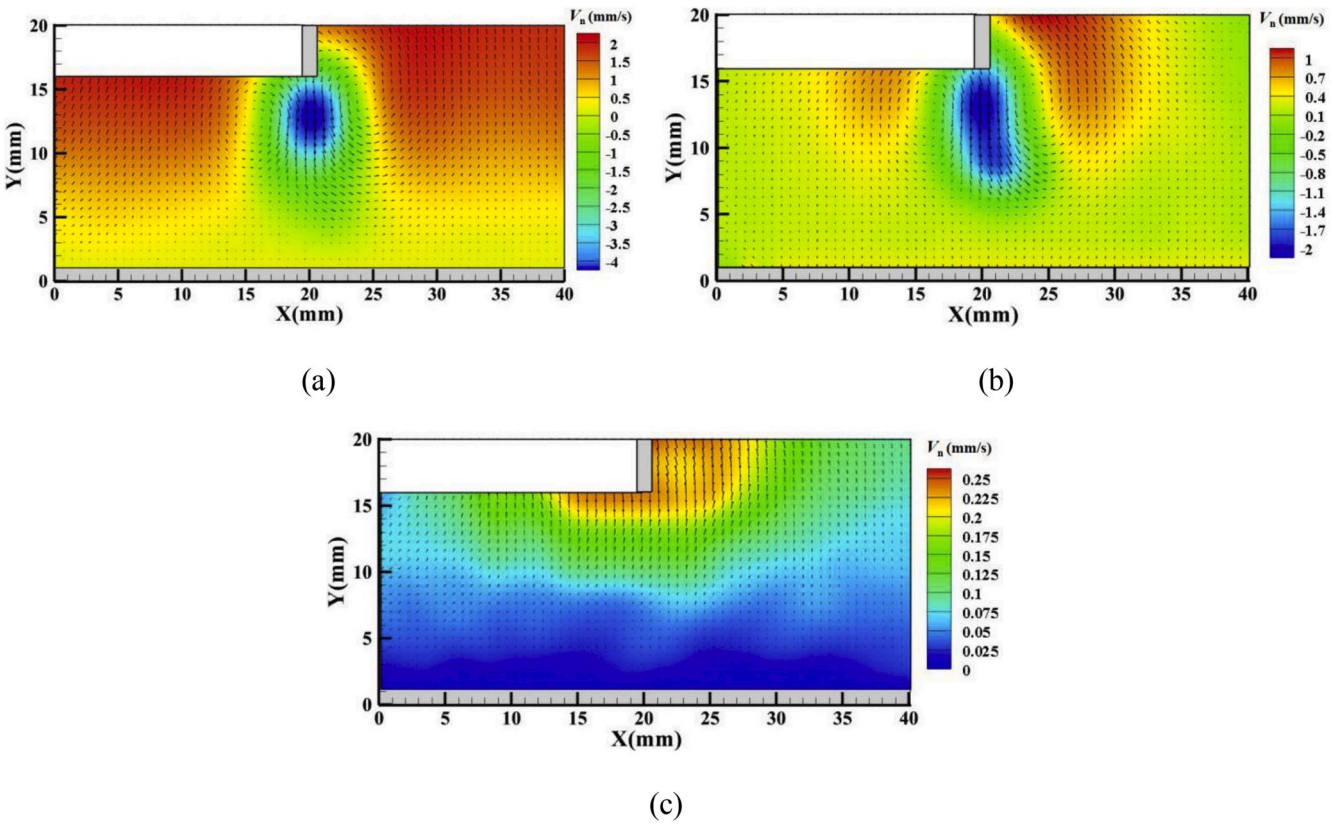

Fig. 13. Velocity field at different frequencies with ±2.0 kV square wave: (a) 5.0Hz, (b) 10.0Hz, (c) 1000.0Hz

electric field to the liquid each time that injection occurs. And it is in the same direction for both polarities. This could produce a net weak flow originated by injection even in the high frequency regime. Note that, the flow motion always directs towards the plate electrode for the injection mechanism.

Secondly, the conduction mechanism applies to AC field with high frequency. Since conduction produces the same amount of positive and negative ions in the bulk, therefore the bulk is electroneutral and the net electric force is applied near the electrodes, not in the bulk. The conduction number C_0, defined as $C_0 = \sigma_0 d/2\varepsilon KE_0$ [32], in our case is quite high (between 10 and 100), so the heterocharge layers near the electrodes are quite small, which explains the observed weak flow motion induced by conduction. Note that, the flow motion always directs towards the needle electrode for the conduction mechanism.

In Fig. 13, we show the velocity field with $f = 5$, 10 and 1000 Hz. For $f = 5$ and 10, the flow moves towards the plate electrode, which means the flow is driven by injection. However, $f = 1000$, we see the flow moving towards the needle electrode. In addition, the flow field is strong in the region very close to the needle while the liquid hardly moves in the region close to the plate. Therefore, we can say that in this case the charge created by conduction dominate over the charge created by injection. Note that in Fig. 13c it seems that the flow always move upwards without backflow. This is mainly due to the limited record area of the PIV data. In addition, the averaging process with the rapidly changing flow field and the possible 3D non-symmetrical flow pattern may also influence the fluid circulation.

4. Concluding remarks

In this study, some preliminary results of electrohydrodynamic flow characteristics of a dielectric liquid (25# transformer oil with 10% cyclohexanol alcohol) in a needle-plate configuration under DC and AC electric field are reported. The curvature of the needle is about 0.1mm and the distance between needle and plate is fixed at 15.0mm. The up to 5.0kV DC voltage and AC square wave voltage of ±2.0kV are applied to the needle electrode.

For the DC case, experimental results show that the current-voltage characteristic curve can be roughly divided into Ohmic and injection regimes. Flow motion driven by the Coulomb force is observed by the PIV technique. For voltage below 0.75kV, the liquid moves towards the needle electrode, and it can be explained by the conduction mechanism. Once the voltage is above 0.75kV, the flow direction reverses and a plume structure is formed, which is due to charge injection. In the conduction regime, the polarity does not influence the intensity of flow motion. However, in the injection regime, the flow is more intense with negative voltage than positive voltage.

For the AC cases, two types of signals with the same 50% duty cycle are considered. It is found that the flow pattern with the AC field is much more complicated than the DC field. For the pulsed voltage (−2.0kV to 0), the flow generally keeps the plume structure, but with smaller maximum velocity amplitude. The reason is mainly due to the time reduction of the electric field's action and charge injection. For the pulsed voltage (0 to+2.0kV), the fluid hardly moves. The reason may be due to the equally important roles played by the injection and conduction mechanisms. For the AC signal (-2.0kV to +2.0kV), the velocity amplitude first decreases along with the increase of frequency and remains a constant value at high frequency. For sufficiently high frequency, the injected charges unable enter into the bulk liquid and a fairly weak flow due to conduction is observed.

Declaration of competing interest

The authors declared that there is no conflict of interest with the following manuscript.

Acknowledgments

This work is supported by National Natural Science Foundation of China (Grant No. 11802079 and 51776054) and CAST-BISEE innovation fund (Grant No. 2019-012). The authors are very grateful to Dr. P. A. Vázquez for various useful discussions, and all the referees are acknowledged for their enlightening suggestions.

References

[1] A. Castellanos, Electrohydrodynamics, Springer, 1998.
[2] A.I. Zhakin, Electrohydrodynamics. Physics-Uspekhi 55 (5) (2012) 465.
[3] A. Castellanos, Coulomb-driven convection in electrohydrodynamics, IEEE Trans. Electr. Insul. 26 (6) (1991) 1201–1215.
[4] J. Seyed-Yagoobi, Electrohydrodynamic pumping of dielectric liquids, J. Electrost. 63 (6–10) (2005) 861–869.
[5] M. Daaboul, P. Traoré, P. Vázquez, et al., Study of the transition from conduction to injection in an electrohydrodynamic flow in blade-plane geometry, J. Electrost. 88 (2017) 71–75.
[6] V.A. Chirkov, S.A. Vasilkov, Y.K. Stishkov, The role of field-enhanced dissociation in electrohydrodynamic flow formation in a highly non-uniform electric field, J. Electrost. 93 (2018) 104–109.
[7] P. Atten, J. Seyed-Yagoobi, Electrohydrodynamically induced dielectric liquid flow through pure conduction in point/plane geometry, IEEE Trans. Dielectr. Electr. Insul. 10 (1) (2003) 27–36.
[8] Y. Feng, J. Seyed-Yagoobi, Understanding of electrohydrodynamic conduction pumping phenomenon, Phys. Fluids 16 (7) (2004) 2432–2441.
[9] P. Atten, Electrohydrodynamic instability and motion induced by injected space charge in insulating liquids, IEEE Trans. Dielectr. Electr. Insul. 3 (1) (1996) 1–17.
[10] D. Testi, Heat transfer enhancement in a dielectric coolant by electroconvection in point-plane geometry, IEEE 20th International Conference on Dielectric Liquids (ICDL) (2019) 1–5.
[11] D. Testi, Heat transfer enhancement by an impinging ionic jet in a viscous transformer coolant, Int. Commun. Heat Mass Tran. 91 (2018) 256–261.
[12] J. Wu, P. Traore, C. Louste, et al., Direct numerical simulation of electrohydrodynamic plumes generated by a hyperbolic blade electrode, J. Electrost. 71 (3) (2013) 326–331.
[13] M. Daaboul, C. Louste, H. Romat, Transient velocity induced by electric injection in blade-plane geometry, J. Electrost. 67 (2–3) (2009) 359–364.
[14] S.A. Vasilkov, V.A. Chirkov, Y.K. Stishkov, Electrohydrodynamic flow caused by field-enhanced dissociation solely, Phys. Fluids 29 (6) (2017), 063601.
[15] M. Becerra, H. Frid, P.A. Vázquez, Self-consistent modeling of laminar electrohydrodynamic plumes from ultra-sharp needles in cyclohexane, Phys. Fluids 29 (12) (2017), 123605.
[16] P. Atten, B. Malraison, M. Zahn, Electrohydrodynamic plumes in point-plane geometry, IEEE Trans. Dielectr. Electr. Insul. 4 (6) (1997) 710–718.
[17] F.M.J. McCluskey, A.T. Perez, The electrohydrodynamic plume between a line source of ions and a flat plate-theory and experiment, IEEE Trans. Electr. Insul. 27 (2) (1992) 334–341.
[18] M. Daaboul, C. Louste, H. Romat, LDV measurements of liquid velocity induced by charge injection in Diesel oil in a blade-plane-slit geometry, J. Phys.: Conference Series. IOP Publishing 142 (1) (2008), 012041.
[19] M. Daaboul, C. Louste, H. Romat, PIV measurements on charged plumes-influence of SiO_2 seeding particles on the electrical behavior, IEEE Trans. Dielectr. Electr. Insul. 16 (2) (2009) 335–342.
[20] C. Louste, H. Romat, P. Traoré, et al., Electroconvective cavity flow patterns created by asymmetric electrode configuration, IEEE Trans. Ind. Appl. 54 (5) (2018) 4851–4856.
[21] Y.K. Stishkov, V.A. Chirkov, Formation of electrohydrodynamic flows in strongly nonuniform electric fields for two charge-formation modes, Tech. Phys. 57 (1) (2012) 1–11.
[22] R. Tobazeon, Electrohydrodynamic instabilities and electroconvection in the transient and AC regime of unipolar injection in insulating liquids: a review, J. Electrost. 15 (3) (1984) 359–384.
[23] P. Atten, B. Malraison, S.A. Kani, Electrohydrodynamic stability of dielectric liquids subjected to ac fields, J. Electrost. 12 (1982) 477–488.
[24] J.S. Cotton, A.J. Robinson, M. Shoukri, et al., AC voltage induced electrohydrodynamic two-phase convective boiling heat transfer in horizontal annular channels, Exp. Therm. Fluid Sci. 41 (2012) 31–42.
[25] S. Rashidi, H. Bafekr, R. Masoodi, et al., EHD in thermal energy systems-A review of the applications, modelling, and experiments, J. Electrost. 90 (2017) 1–14.
[26] D. Nakhla, E. Thompson, B. Lacroix, et al., Measurement of heat transfer enhancement in melting of n-Octadecane under gravitational and electrohydrodynamics (EHD) forces, J. Electrost. 92 (2018) 31–37.
[27] C. Gouriou, P. Traoré, C. Louste, Influence of seeding particle type on velocity measurements in silicone oil under high voltage, IEEE Trans. Ind. Appl. 53 (3) (2017) 2471–2476.
[28] R. Hosseini, A. Takemura, An objective look at obtaining the plotting positions for QQ-plots, Commun. Stat. Theor. Methods (2015) 4716–4728.
[29] M. Daaboul, C. Louste, H. Romat, PIV measurements of the influence of seeding particles concentration on the velocity of an EHD flow, in: ESA/IEEE-IAS/IEJ/SFE Joint Conference on Electrostatic, 2009.
[30] A.T. Perez, P.A. Vazquez, A. Castellanos, Dynamics and linear stability of charged jets in dielectric liquids, IEEE Trans. Ind. Appl. 31 (4) (1995) 761–767.
[31] Y. Sha, Y. Zhou, D. Nie, et al., A study on electric conduction of transformer oil, IEEE Trans. Dielectr. Electr. Insul. 21 (3) (2014) 1061–1069.
[32] P.A. Vázquez, M. Talmor, J. Seyed-Yagoobi, et al., In-depth description of electrohydrodynamic conduction pumping of dielectric liquids: Physical model and regime analysis, Phys. Fluids 31 (11) (2019), 113601.